doi:10.1093/brain/awaa227

BRAIN
A JOURNAL OF NEUROLOGY

Connexins in neuromyelitis optica: a link between astrocytopathy and demyelination

Chloé Richard,[1] Anne Ruiz,[1] Sylvie Cavagna,[1] Maxime Bigotte,[1] Sandra Vukusic,[2,3] Katsuhisa Masaki,[4] Toshihiko Suenaga,[5] Jun-Ichi Kira,[4] Pascale Giraudon[1] and Romain Marignier[1,2,3]

Neuromyelitis optica, a rare neuroinflammatory demyelinating disease of the CNS, is characterized by the presence of specific pathogenic autoantibodies directed against the astrocytic water channel aquaporin 4 (AQP4) and is now considered as an astrocytopathy associated either with complement-dependent astrocyte death or with astrocyte dysfunction. However, the link between astrocyte dysfunction and demyelination remains unclear. We propose glial intercellular communication, supported by connexin hemichannels and gap junctions, to be involved in demyelination process in neuromyelitis optica. Using mature myelinated cultures, we demonstrate that a treatment of 1 h to 48 h with immunoglobulins purified from patients with neuromyelitis optica (NMO-IgG) is responsible for a complement independent demyelination, compared to healthy donors' immunoglobulins ($P < 0.001$). In parallel, patients' immunoglobulins induce an alteration of connexin expression characterized by a rapid loss of astrocytic connexins at the membrane followed by an increased size of gap junction plaques (+60%; $P < 0.01$). This was co-observed with connexin dysfunction with gap junction disruption (–57%; $P < 0.001$) and increased hemichannel opening (+17%; $P < 0.001$), associated with glutamate release. Blocking connexin 43 hemichannels with a specific peptide was able to prevent demyelination in co-treatment with patients compared to healthy donors' immunoglobulins. By contrast, the blockade of connexin 43 gap junctions with another peptide was detrimental for myelin (myelin density –48%; $P < 0.001$). Overall, our results suggest that dysregulation of connexins would play a pathogenetic role in neuromyelitis optica. The further identification of mechanisms leading to connexin dysfunction and soluble factors implicated, would provide interesting therapeutic strategies for demyelinating disorders.

1 INSERM U1028, CNRS UMR 5292, Lyon1 University, Center for Research in Neuroscience of Lyon, Lyon, France
2 Service de neurologie, sclérose en plaques, pathologies de la myéline et neuro-inflammation, Hôpital Neurologique Pierre Wertheimer Hospices Civils de Lyon, Lyon, France
3 Centre de référence des maladies inflammatoires rares du cerveau et de la moelle, Lyon, France
4 Department of Neurology, Neurological institute, Graduate School of Medical Sciences, Kyushu University
5 Department of Neurology, Tenri hospital, Tenri, Japan

Correspondence to: Romain Marignier, MD, PhD
Centre de référence des maladies inflammatoires rares du cerveau et de la moelle
Service de neurologie, sclérose en plaques, pathologies de la myéline et neuro-inflammation
Hôpital Neurologique Pierre Wertheimer
59 boulevard Pinel, 69677 Bron cedex, France
E-mail: romain.marignier@chu-lyon.fr

Keywords: connexins; demyelination; neuromyelitis optica; astrocyte

Abbreviations: DIV = day in vitro; NMO = neuromyelitis optica

Received February 21, 2019. Revised April 1, 2020. Accepted May 6, 2020

Introduction

Neuromyelitis optica (NMO) is a rare neuroinflammatory demyelinating disease of the CNS that is considered an autoimmune astrocytopathy (Kira, 2011; Ratelade and Verkman, 2012; Jacob *et al.*, 2013). Indeed, NMO is characterized by the presence of autoantibodies (NMO-IgG) directed against the astrocytic water channel aquaporin 4 (AQP4) and playing a key role in NMO physiopathology (Lennon, 2005). NMO is a complex disease involving several pathological mechanisms, as suggested by the presence of six types of lesions referenced in patients (Misu *et al.*, 2013) such as: complement-dependent cell toxicity (Saadoun *et al.*, 2010), cytokine-mediated inflammation (Bradl *et al.*, 2009), inflammatory cell-mediated response (Bennett *et al.*, 2009) and autoantibody-mediated astrocytopathy (Hinson *et al.*, 2010; Marignier *et al.*, 2010, 2016). This later mechanism is of particular importance in NMO. Given the context of autoimmune astrocytopathy, an antibody targeting a membrane protein can induce its internalization or intracellular signalling, leading to a modification of physiological cellular functions (Brimberg *et al.*, 2015). We previously showed that NMO-IgG induced, in association with AQP4 internalization, an alteration of membrane expression of glutamate transporters on astrocytes associated with increased levels of extracellular glutamate (Marignier *et al.*, 2010, 2016). These alterations were co-observed in an original rat model of NMO with myelin and axonal loss but the direct link between astrocytopathy and demyelination remained unclear.

Astrocytes are abundant glial cells known to be key elements in the maintenance of CNS homeostasis. Most astrocytic essential functions depend on the formation of a neuroglial network, established and maintained by connexins (Abrams and Rash, 2009). Connexins are transmembrane molecules assembling in hexameric units called connexons, forming hemichannels, unopposed connexons, or gap junction channels by the docking of two connexons and these channels aggregate to form gap junction plaques. Those two functions allow, respectively, exchanges with the extracellular medium or quick cell-to-cell passage of small metabolites and ions (e.g. ATP, glutamate, D-serine, calcium) less than ~1 kDa (Abrams and Rash, 2009; Giaume *et al.*, 2013). Several types of connexins (Cx) are expressed in the CNS and their expression is particularly high in astrocytes, which mainly express Cx43 and Cx30, and to a lesser extent Cx26. Astrocytes are highly connected by gap junctions. Oligodendrocytes also express a different set of connexins composed of Cx47, Cx32 and Cx29 and can form gap junctions with astrocytes. Glial connexins have many roles such as intercellular signalling, via calcium wave propagation, exchange of metabolites and gliotransmission, essential for neuronal functioning (Giaume and Venance, 1998; Giaume *et al.*, 2013). Moreover, connexins are actively implicated in myelin formation and integrity since they sustain a dialogue between astrocytes, oligodendrocytes and neurons (Cotrina and Nedergaard, 2012; Nualart-Marti *et al.*, 2013; Li *et al.*, 2014; Niu *et al.*, 2016). Connexin expression and gap junction channel and hemichannel functions are highly regulated under physiological conditions and can be altered under pathological conditions by a decrease of extracellular calcium levels, proinflammatory cytokines or post-translational modifications (Retamal *et al.*, 2007; Giaume *et al.*, 2013; Orellana *et al.*, 2013; Solan and Lampe, 2014; Su and Lau, 2014).

Connexin alterations, especially astrocytic Cx43, have been identified and linked to the severity of the disease in multiple sclerosis and NMO (Masaki *et al.*, 2013). Moreover, a functional link between AQP4 and Cx43 has been identified, supporting the hypothesis of a connexinopathy induced by autoantibodies directed against AQP4 in NMO (Nicchia *et al.*, 2005). All those observations led us to hypothesize that a disruption of intercellular communications could be one mechanism explaining the link between astrocytopathy and demyelination in the setting of NMO. In this study we proposed to evaluate the potential involvement of connexins in demyelination induced by NMO-IgG.

Materials and methods

Patient samples and IgG purification

Plasmapheresis of 10 patients from the French cohort NOMADMUS, diagnosed as NMO spectrum disorder (Wingerchuk *et al.*, 2015) were selected from NeuroBioTec biobank (Lyon University Hospital). Eight patients tested positive for anti-AQP4 immunoglobulin of type G (IgG) and negative for anti-myelin oligodendrocyte glycoprotein (MOG) IgG, on a cell-based assay. One patient tested positive for anti-MOG autoantibodies and negative for anti-AQP4 autoantibodies. One patient tested negative for both anti-AQP4 and anti-MOG autoantibodies. IgG purification was performed as previously described (Marignier *et al.*, 2010, 2016). NMO-IgGs purified from different patients were termed NMO1 to NMO10; Patients NMO1–NMO8 tested positive for anti-AQP4 autoantibodies, Patient NMO9 was double seronegative and Patient NMO10 tested positive for anti-MOG autoantibodies. Sera from four healthy donors were collected from 'Etablissement Français du Sang' and tested negative for anti-AQP4 IgG. Purified IgG from healthy donors were termed as CTRL-IgG. IgG purification was performed as previously described (Marignier *et al.*, 2010, 2016). NMO-IgGs and CTRL-IgGs were used individually or pooled for cell treatment.

AQP4-IgG depletion

Anti-AQP4 antibody depletion was performed as previously described (Marignier *et al.*, 2016). Briefly, HEK-293 cells stably transfected with human AQP4-M23 plasmid were seeded in six-well plates at a density of 10^6 cells. IgG AQP4$^+$ was added in each well for 20 min at 37°C, CO_2 atmosphere and gentle rotation. Contact with cells was performed six times to deplete IgG directed against AQP4. Adsorbed IgG were termed NMOdep.

Cell culture

Mixed glial cell and astrocytic cultures

Primary mixed glial cell cultures were obtained from cortices of 1-day-old rat pups; microdissection and mechanical disruption were done as previously described (Marignier *et al.*, 2010, 2016). To obtain a pure culture of astrocytes, cells were treated with 1 µM of cytosine arabinoside on day *in vitro* (DIV) 8 and DIV13. Cells were kept for 18 to 22 days before treatment and were used for morphological and biochemical studies.

Myelinating culture

Primary myelinated cultures were obtained from Day 15 embryonic rat spinal cord as previously described (Thomson *et al.*, 2008). Briefly, plates and culture chambers were coated with poly-L-lysine (13 µg/ml in sterile water). Cortical astrocytes, from pure astrocyte culture as described above, were detached with Accutase® solution (Sigma A6964) and resuspended in glial cell culture medium at a density of 200 000 cells/ml. These astrocytes were left to attach for 5 days before myelinating culture plating and were used to improve myelination as described previously (Sorensen *et al.*, 2008). Following dissection of embryonic spinal cords, mechanic and enzymatic dissociation, cells were counted, and final volume was adjusted to obtain 700 000 cells/ml in plating medium [Dulbecco's modified Eagle medium (DMEM) 1 g/l glucose supplemented with 1% penicillin streptomycin, 25% horse serum, 25% Hanks' balanced salt solution (HBSS)]. Next, 200 000 cells per chamber or 400 000 cells per well, were left to attach for at least 2 h at 37°C with 5% CO_2. Finally, differentiation medium (DMEM GlutaMAX™ 4.5 g/l glucose supplemented with 1% penicillin streptomycin, 0.5% N2 supplement (ThermoFisher 1750258), 10 ng/ml biotin, 50 nM hydrocortisone, 10 µg/ml insulin) was added in a proportion of 40% of total volume. Half the culture medium was carefully replaced three times a week and insulin was omitted from culture medium after DIV12. Cells were kept from DIV14 to DIV28 and treated at DIV26 when myelination was optimum (Supplementary Fig. 1L–N), to be used for biochemical and morphological studies.

Cell treatments

Cultures were treated for 1 h to 48 h with either culture medium (no treatment condition) or purified IgG from healthy donors (CTRL-IgG) or from patients with NMO (NMO-IgG) at a concentration of 0.4 mg/ml. For connexin activity examination, treatments with connexin modulators were used: carbenoxolone (50 µM) was applied 5 min before dye uptake and scrape loading assays; GAP27, a specific mimetic peptide targeting the Cx43 extracellular loop (sequence SRPTEKTIFII) and blocking Cx43 gap junction channels and hemichannels (Evans and Leybaert, 2007) was applied 60 min before scrape loading assay; lipopolysaccharide (LPS) at 10 ng/ml was applied 24 h before dye uptake assay to induce hemichannels opening (De Vuyst *et al.*, 2007). To test the implication of connexins in demyelination, we co-treated myelinated cultures with GAP19 (344 µM), a mimetic peptide specific of Cx43 intracellular loop (sequence KQIEIKKFK) blocking specifically Cx43 hemichannels (Abudara *et al.*, 2014), together with no treatment, CTRL-IgG or NMO-IgG for 48 h or we treated myelinated cultures with GAP27 alone (260 µM) for 48 h. GAP19 and GAP27 peptides were synthetized by Pepnome Inc. with a purity of 95%.

Immunocytochemistry

Immunocytochemistry (ICC) labelling of cultured cells was performed as described before (Marignier *et al.*, 2010) (Supplementary Table 1). For myelination evaluation, myelin basic protein (MBP) and phosphorylated neurofilament (pNF) were co-labelled at DIV28 after 48 h treatment. Twenty fields per condition and per experiment were taken, by investigators blinded for treatment condition, with a fluorescent microscope equipped with epifluorescence (Axio Imager Z1 apotome technology, Zeiss). Image analysis was performed using ImageJ software. The density of myelinated axons was performed by measuring the area fraction represented by MBP or pNF immunoreactivity and making the ratio of the amount of MBP on pNF. The length of myelinated segments was also measured using the segmented line tool of ImageJ.

Transmission electron microscopy

Transmission electron microscopy (TEM) was performed at the CIQLE facilities (Centre d'Imagerie Quantitative Lyon-Est) as described before (Marignier *et al.*, 2016) on myelinated cultures. Approximately 20 fields per condition were taken to examine gap junction plaques, characterized by a specific aspect in TEM with a reduced intercellular space of ~2–4 nm. Gap junction channels plaque size was evaluated using the segmented line tool of ImageJ software.

Cell fractioning assay and western blot analysis

Membrane fraction of cultured astrocytes was isolated using the ProteoExtract® subcellular proteome extraction kit (Calbiochem 539790) and following user protocol. Briefly, cells were detached using Accutase® solution and centrifuged at 300*g* for 5 min. Then cell pellets were washed trice by addition of washing buffer followed by 5 min incubation on a wheel and 10 min centrifugation at 300*g* at 4°C. For membrane fraction extraction (cell membrane and organelles), pellets were resuspended in buffer number 2 containing protease and phosphatase inhibitors, incubated 30 min at 4°C on a wheel and centrifuged at 5500*g* 10 min at 4°C. Supernatant was harvested and kept at −80°C aliquoted. Then immunoblot (western blot) was performed on membrane fraction as described before (Varrin-Doyer *et al.*, 2012; Marignier *et al.*, 2016). Briefly, proteins were separated on SDS-PAGE gels and transferred on nitrocellulose membrane. Then immunodetection was performed with specific primary antibodies (for dilution see Supplementary Table 1) and anti-IgG secondary antibodies coupled with horseradish peroxidase (HRP). Proteins were revealed using a chemiluminescence assay and signal analysis was performed by measuring band density using ImageJ software.

Gap junction function

Gap junction channel coupling was assessed with scrape loading dye transfer technic performed as described previously (Retamal *et al.*, 2007) on myelinated cultures. Briefly, cells were washed in HEPES solution containing (in mM): 150 NaCl, 5.4 KCl, 1 $MgCl_2$, 5 HEPES, 10 glucose and 2.4 $CaCl_2$, for 5 min. Then cells were washed in calcium-free HEPES solution for 1 min. Fluorescent dye Lucifer yellow (Sigma 10259, 1 mg/ml in calcium-free HEPES solution) was added and scrape loading was performed using a 23-gauge needle. After 1 min, Lucifer yellow dye was washed out three times in HEPES solution and after 8 min, acquisition of 10 fields per condition was performed with

fluorescent microscope equipped with epifluorescence (Axio Imager Z1 apotome technology, Zeiss) and AxioVision Rel 4.8 software. Image analysis was performed using ImageJ to determine Lucifer yellow fluorescent dye diffusion area, expressed in arbitrary units.

Hemichannel function

Hemichannel opening was determined using dye uptake of ethidium bromide (EtBr). First, cells were washed in HBSS (in mM: 137 NaCl, 5.4 KCl, 0.34 Na_2HPO_4, 0.44 KH_2PO_4, 1.2 $CaCl_2$; pH 7.4) then EtBr 0.5 µM was applied for 10 min at 37°C. After three washes in HBSS, cells were fixed with 4% PFA for 10 min at room temperature and washed three times in PBS. DAPI solution was used for nucleus staining (0.1 µg/ml) was incubated 5 min before cells were mounted in fluoropreserve® (Millipore) and examined with confocal microscope Leica SP5 (518 nm excitation and 605 nm emission). Images were then analysed using ImageJ software to evaluate nuclear fluorescence corresponding to EtBr fixation.

Data collection and statistical analysis

Statistical analyses and graphs were established using GraphPad Prism 5.0. Data on graphs are presented as bars of mean with standard error of the mean (SEM) or by box and whiskers representing minimum to maximum values and mean with a plus symbol. Normality of distribution and equality of variances was evaluated using respectively D'Agostino-Pearson and Bartlett's tests before statistical analysis to choose the appropriate parametric or non-parametric test to compare conditions. For multiple conditions comparison, we used either an ANOVA or Kruskal-Wallis test followed by Dunn's *post hoc* test. For all tests, alpha risk was fixed at 5% so differences were considered significant for $P < 0.05$. Levels of significance are indicated as: $^{*}P < 0.05$, $^{**}P < 0.01$, $^{***}P < 0.001$.

Data availability

The data that support the findings of this study are available from the corresponding author, upon reasonable request.

Results

NMO-IgG induce demyelination in a myelinated culture model

To assess the implication of NMO-IgG in demyelination, we developed a myelinated culture composed of glial cells (astrocytes, oligodendrocytes and microglial cells) and neurons with myelinated axons. The quality of the culture was validated by labelling myelinated axons with MBP and pNF and presented nodes of Ranvier expressing neurofascin (NFASC) (Supplementary Fig. 1A and C). In addition, compaction of myelin was checked by electron microscopy (Supplementary Fig. 1B). The presence of neuronal synapses (Supplementary Fig. 1D), astrocytes (Supplementary Fig. 1E and F), oligodendrocytes mature and precursors (Supplementary Fig. 1F and G) and the presence of astrocytic and oligodendrocytic connexins (Supplementary Fig. 1O and P) was assessed by immunofluorescence labelling. The presence of astrocyte, oligodendrocyte, myelin and neuronal protein was also assessed by western blot (Supplementary Fig. 1Q). At DIV26, cultures were treated either with culture medium (no treatment), or purified IgG from healthy donors (CTRL-IgG) or from NMO patients (NMO-IgG) for 48 h. NMO-IgG termed NMO1–7 tested positive for anti-AQP4 and negative for anti-MOG autoantibodies, NMO9 tested negative for both anti-AQP4 and anti-MOG autoantibodies and NMO10 tested positive for anti-MOG and negative for anti-AQP4. We also used a condition with NMO-IgG depleted in anti-AQP4 IgG (NMOdep) as a control. The co-labelling of myelinated axons with MBP and pNF (Fig. 1A) allowed myelin quantification. Myelin density (Fig. 1B), expressed as the ratio of MBP on pNF immunoreactivities, was decreased by 34%, 39%, 52%, 60%, 45%, 58%, 68% by NMO1–7 compared to CTRL-IgG ($P < 0.001$), and by 35% by NMO9 compared to CTRL-IgG ($P < 0.01$). NMO10 and NMOdep did not significantly change myelin density compared to CTRL-IgG or no treatment conditions. To evaluate the effect of NMO-IgG on myelin integrity further, we measured the length of myelinated segments (Fig. 1C), expressed in micrometres, which was strongly decreased by 26%, 23%, 32%, 46%, 28% and 38% by NMO1, 2, 4, 5, 6 and NMO7, respectively, compared to CTRL-IgG ($P < 0.01$ and $P < 0.001$). NMO3, NMO9, NMO 10 and NMOdep did not show significant differences compared to CTRL-IgG ($P > 0.05$). Finally, the density of axons, determined using the fraction area of pNF immunoreactivity, was only decreased by NMO4 and NMO10 compared to no treatment (Fig. 1D: –40% $P < 0.01$). The choice of DIV26 to treat with NMO-IgG was made because we studied myelination over time and found that it was optimum from DIV26. In fact, we performed co-labelling of MBP and pNF from DIV14 to DIV28 and showed that myelin density and myelin segment length increased over time but reached a maximum at DIV26 with no further increase at DIV28 (Supplementary Fig. 1L–N). We also checked the effect of NMO-IgG on MOG (Supplementary Fig. 1H and I) with a co-labelling with pNF and showed a decrease of myelinated segment length induced by NMO-IgG compared to CTRL-IgG and no treatment conditions. We checked that astrocyte were preserved in the culture by labelling GFAP which immunoreactivity is not altered after 48 h treatment with NMO-IgG (Supplementary Fig. 1J and K). In addition, the number of microglial cells labelled with Iba1 was increased after NMO-IgG treatment (data not shown).

NMO-IgG induces a dynamic modification of Cx43 membrane expression

Our hypothesis was that, by targeting AQP4 on astrocytes, NMO-IgG could induce connexin alteration and lead to

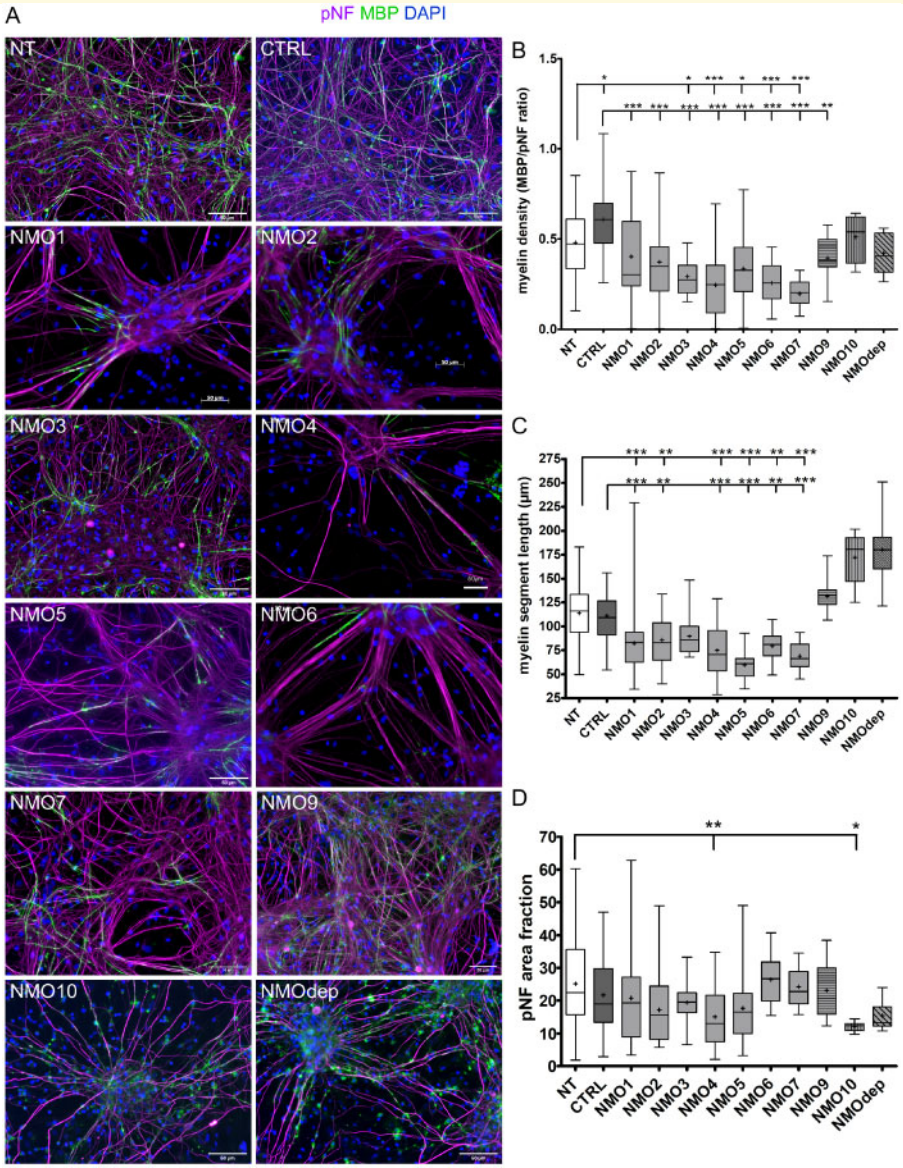

Figure 1 Demyelination is induced by NMO-IgG without complement addition. (**A**) Co-immunolabelling with the myelin marker MBP (in green) and axon marker phosphorylated neurofilament (pNF, in magenta) after 48 h treatment with culture medium (no treatment, NT), CTRL-IgG (CTRL) or NMO-IgGs (from nine different NMO patients: NMO1–7, 9 and 10) or NMO-IgG depleted in anti-AQP4 autoantibodies (NMOdep) (**B**) Myelinated axon density, expressed by the ratio of the amount of MBP on pNF area fraction, is strongly decreased by NMO3–7 and increased by CTRL when compared to no treatment. NMO1–7 and NMO9 strongly decrease myelin density when compared to CTRL. (**C**) Myelinated segment length is strongly decreased by NMO1, 2 and 4–7 compared to no treatment and CTRL. (**D**) The pNF area fraction is only decreased by NMO4 compared to no treatment. Box and whiskers represent median and interquartile range (IQR) with minimum and maximum values; the plus symbol indicates mean; Kruskal-Wallis analysis and Dunn's *post hoc* test $*P < 0.05$, $**P < 0.01$, $***P < 0.001$; $n = 4$ cultures, each condition in duplicate.

subsequent demyelination. We first focused on Cx43, the main astrocytic connexin, and assessed its expression in glial cell culture with co-immunolabelling Cx43 and AQP4 after 1 h or 24 h treatment with CTRL-IgG or NMO-IgG (NMO: pool of igG from three patients; Fig. 2A). Results showed that NMO-IgG induced an increase in AQP4 particle size and the partial co-localization of AQP4 and Cx43 after 1 h treatment (higher magnification). The co-labelling Cx43 and Rab11, an endosomal marker, showed a partial co-localization after 1 h treatment with NMO-IgG and not with CTRL-IgG (Fig. 2B). After 24 h, NMO-IgG increased Cx43 particle size and this was associated with a decrease of AQP4 immunoreactivity (higher magnification). To quantify this alteration, we performed a particle analysis of Cx43 (Fig. 2D) particle size showing an increase in Cx43 particle size induced by NMO-IgG compared to no treatment

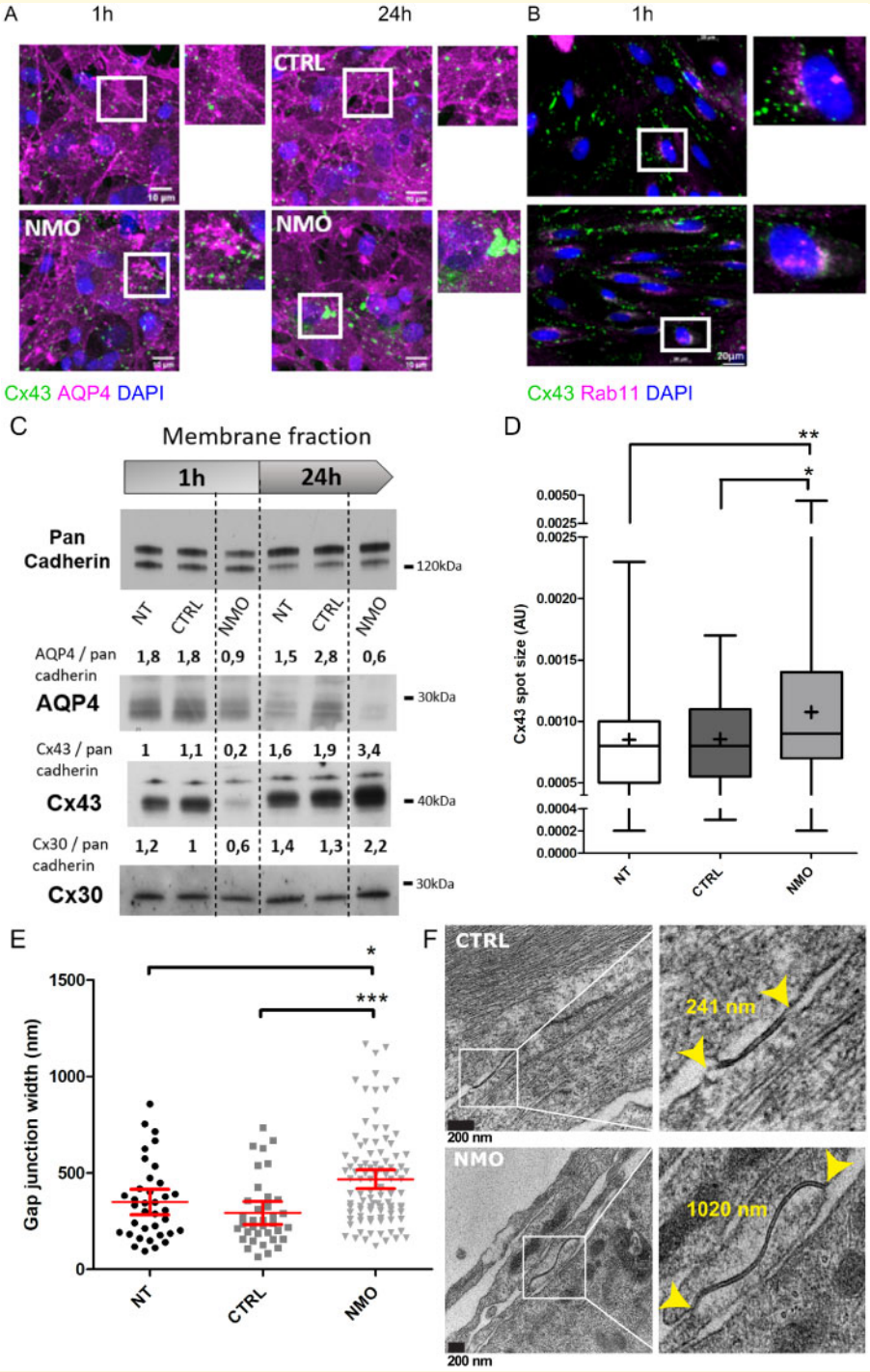

Figure 2 Astrocytic Cx43 membrane expression is altered by NMO-IgG. (**A**) Confocal microscope imaging of Cx43 and AQP4 co-immunolabelling after 1 h or 24 h treatment of a glial cell culture with CTRL-IgG (CTRL) or NMO IgG (NMO: from a pool of IgG from Patients NMO1–3) showing an increase of Cx43 spot size and a decrease of AQP4 immunoreactivity induced by NMO-IgG after 24 h. (**B**) Co-immunolabelling of Cx43 and endosomal marker Rab11 in an astrocytic culture showing partial co-localization of Cx43 and Rab11 around nuclei after 1 h treatment with NMO-IgG. (**C**) Connexins expression in astrocyte using cell fractioning and western blot analysis of membrane/organelle fraction after 1 h or 24 h treatment with no treatment (NT), CTRL-IgG (CTRL) and NMO-IgG (NMO: from a pool of IgG from Patients NMO1–3). Pan-cadherin is a loading control for membrane/organelle fraction that was used to perform a semi-quantitative analysis of AQP4, Cx43, phosphorylated Cx43 (on Ser368) and Cx30 expressions (ratio above bands). AQP4, Cx43, pCx43 and Cx30 expression are decreased after 1 h in NMO condition compared to CTRL. After 24 h, AQP4 expression is still decreased whereas Cx43, pCx43 and Cx30 expressions are increased in NMO condition compared to CTRL. (**D**) Analysis of Cx43 spot size after 24 h treatment with no treatment, CTRL-IgG (CTRL) and NMO-IgG (NMO: summative data of Patients NMO1, 2, 4 and 5 IgG) in a myelinated culture showing increased Cx43 spot size in NMO condition compared to CTRL and no treatment conditions. (**E**) Measurement of gap junction plaque size on electron microscopy pictures after 24 h treatment

(continued)

(+26.4%, $P < 0.01$) and CTRL-IgG (+25.6% $P < 0.05$). We also performed a cell fractioning assay on an astrocytic culture to study the expression of AQP4, and astrocytic connexins Cx43 and Cx30 after either 1 h or 24 h treatment with no treatment, CTRL-IgG or NMO-IgG (NMO: pool of IgG from three patients). We analysed their expression in the membrane fraction (comprising cell membrane and organelles) by western blot (Fig. 2C). Pan-cadherin was used as loading control to perform a semi-quantitative analysis of AQP4, Cx43, phosphorylated Cx43 on Serine 368 (pCx43) and Cx30 expressions (ratio above bands). AQP4, Cx43, pCx43 and Cx30 expression in the membrane fraction are decreased by 50%, 82% and 40%, respectively, after 1 h treatment with NMO-IgG compared to CTRL-IgG. After 24 h, AQP4 expression is still decreased by 79% while Cx43, pCx43 and Cx30 expressions are increased by 79%, 71% and 69%, respectively, by NMO compared to CTRL-IgG. We then evaluated the presence and the size of gap junction plaques between astrocytes by electron microscopy in a myelinated culture treated 24 h with either no treatment, CTRL-IgG or NMO-IgG (Fig. 2E and F: summative data from three NMO patients' IgG). Astrocytes were identified by the abundance of filaments and by the light grey colour of their cytoplasm. Gap junction plaque size was increased by NMO-IgG (+60%, $P < 0.01$) when compared to CTRL-IgG (Fig. 2E). Altogether, these results show a quick subcellular reorganization of AQP4 and Cx43 induced by NMO-IgG, followed by AQP4 loss and increase of Cx43 and Cx30 at cell membrane, associated with larger size of gap junction plaque.

NMO-IgG induces connexin dysfunction

Since altered expression of connexin could lead to its dysfunction, we studied gap junction and hemichannel function in glial cultures. Gap junction function was assessed by performing scrape loading dye transfer technic on a myelinated culture treated 24 h in no treatment, CTRL-IgG or NMO-IgG conditions (Fig. 3A). We measured the area of diffusion of Lucifer yellow (a fluorescent dye crossing from one cell to another through gap junctions; Fig. 3A), reflecting the amount of gap junction coupling between cells. Dye diffusion area was decreased by NMO-IgG (–57% NMO: summative data of two pools of three patients' IgG, $P < 0.001$) compared to CTRL-IgG after 24 h treatment (Fig. 3B). To make sure of the implication of connexins, we blocked either all connexins using carbenoxolone or specifically Cx43 gap junctions using the mimetic peptide GAP27, and found, respectively, a drastic reduction of dye diffusion (–83% $P < 0.001$ compared to CTRL-IgG) and a decrease of dye diffusion (–44% $P < 0.001$ compared to CTRL-IgG) comparable to NMO-IgG condition ($P > 0.05$). We also used an astrocytic culture to study connexins gap junction coupling and showed similar results with decreased dye diffusion area induced by NMO-IgG (IgG from Patients NMO1 and NMO2) compared to CTRL-IgG and no treatment after 24 h treatment (Fig. 3C and D). We also used LPS, a bacterial component known to induce inflammation and reduce gap junction coupling (Retamal *et al.*, 2007), that also decreased dye diffusion area compared to no treatment and CTRL-IgG. Likewise, GAP27, also induced a similar effect to NMO-IgG. We then focused on astrocytic Cx43 and oligodendrocytic Cx47 as they form heterotypic gap junctions between astrocyte and oligodendrocytes. In the myelinated cultures, Cx43–Cx47 gap junctions, showed by the presence of a partial co-localization with confocal microscopy, were strongly decreased by NMO-IgG (Fig. 3E).

We also studied hemichannel function and performed EtBr uptake assay on a glial cell culture treated 24 h with no treatment, CTRL-IgG or NMO-IgG. To validate hemichannel functionality in our cell models, we used LPS to induce hemichannel opening and carbenoxolone to block connexins. EtBr fluorescence was measured in each nucleus of astrocytes (Fig. 3F). EtBr uptake in astrocytes was increased by NMO-IgG (NMO: summative data of two pools of three patients' IgG) and LPS compared to CTRL-IgG (Fig. 3G). As expected, carbenoxolone had no effect compared to no treatment and CTRL-IgG. To ensure that increase of EtBr uptake was not due to cell death, we performed propidium iodide assay of cell death by flow cytometry and showed comparable number of dead cells in NMO-IgG (7.21%), CTRL-IgG (9.65%) and no treatment (10.9%) conditions after 24 h treatment (Supplementary Fig. 2A). A study of the release of glutamate in the supernatant of mixed glial cell culture showed a transient increase in glutamate release after 10 min induced by NMO-IgG (summative data of four patients' IgG) compared to CTRL-IgG (Supplementary Fig. 2B). This glutamate release was strongly reduced by carbenoxolone in both conditions demonstrating the involvement of connexins in glutamate release. Altogether these results show a severe alteration of glial connexin gap junction and hemichannel functions under NMO-IgG treatment that could be responsible for a toxic microenvironment and participate in NMO-IgG induced demyelination.

Figure 2 Continued

with no treatment, CTRL-IgG (CTRL) and NMO-IgG (NMO: summative data of Patients NMO2, 4 and 5 IgG) showing an increase in NMO condition compared to no treatment and CTRL. (**F**) Electron microscopy imaging of gap junction plaques (delimited by yellow arrows) in a myelinated culture after 24 h treatment with CTRL-IgG (CTRL) or NMO-IgG (NMO: NMO4 chosen for illustration). Box and whiskers represent median value with IQR and minimum maximum values; mean is represented by a plus symbol. Scatter dot plot represent median value with IQR. Kruskal-Wallis ANOVA and Dunn's *post hoc* test $^{*}P < 0.05$, $^{**}P < 0.01$; $n = 1$ culture for immunofluorescence assays, $n = 2$ independent experiments for electron microscopy, $n = 1$ experiment for western blot.

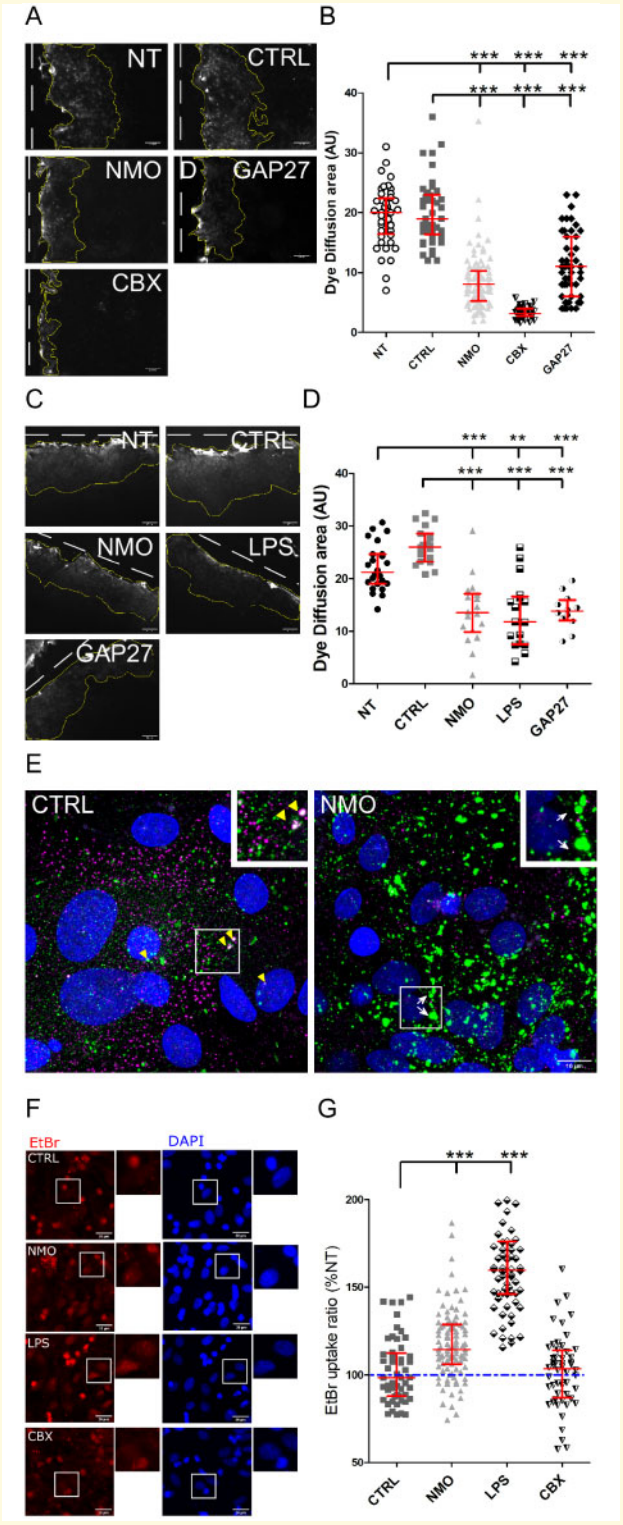

Figure 3 Gap junctional coupling decrease and hemichannel opening are induced by NMO-IgG. (**A**) Fluorescence images of scrape loading dye transfer assay showing Lucifer yellow diffusion (area delimited by yellow line) from the scrape (white dot line) in a myelinated culture treated 24 h with either no treatment (NT), CTRL-IgG (CTRL) or NMO-IgG (NMO) or treated 5 min with connexin inhibitor carbenoxolone (CBX 50 μM); or treated 30 min with GAP27, a mimetic peptide blocking Cx43 gap junction channel. (**B**) Dye diffusion area is strongly decreased in NMO (summative data of two pools of IgG from Patients NMO1–3 and NMO4–6) and GAP27 conditions and is almost abolished by carbenoxolone compared to CTRL and no treatment conditions ($n = 2$ cultures with each condition in duplicate). (**C**) Fluorescence images of scrape loading dye transfer assay showing Lucifer yellow diffusion (area delimited by yellow line) from the scrape (white dot line) in an astrocytic culture treated 24 h with either no treatment, CTRL-IgG (CTRL) or NMO-IgG (NMO) or lipopolysaccharide (LPS) a bacterial component inducing inflammation, or treated 30 min with GAP27. (**D**) Dye diffusion area is strongly decreased in NMO (summative data of IgG from Patients NMO1 and 2), GAP27 and LPS conditions compared CTRL and no treatment conditions ($n = 1$ culture). (**E**) Confocal image of co-immunofluorescent labelling of Cx43 and Cx47 in a myelinated culture model showing the presence of Cx43-Cx47 gap junctions in CTRL-IgG condition after 24 h treatment (yellow arrowheads). NMO-IgG induce an increase of Cx43 spot size (white arrows) and a disruption of Cx43-Cx47 gap junctions. (**F**) Confocal microscopy imaging of EtBr (red) and DAPI (blue) after EtBr uptake experiment in mixed glial cells treated 24 h with no treatment, CTRL-IgG (CTRL), NMO-IgG (NMO) or lipopolysaccharide (LPS) or 5 min with carbenoxolone (50 μM). (**G**) Measurement of EtBr immunoreactivity in astrocyte nuclei showing an increase induced by NMO (Summative data of two pools of IgG from Patients NMO1–3 and NMO4–6) and LPS conditions compared to CTRL. EtBr uptake is expressed as a percentage of no treatment condition showed by the dotted red line ($n = 1$ culture with each condition in duplicate). Bars represent mean values ± SEM. Kruskal-Wallis analysis of variances and Dunn's *post hoc* analysis ***$P < 0.001$.

Blockade of Cx43 hemichannels prevents NMO-IgG-induced demyelination

To test the direct implication of connexin alteration on demyelination induced by NMO-IgG, we treated myelinated cultures for 48 h with either no treatment, CTRL-IgG or NMO-IgG or those three conditions co-treated with the mimetic peptide GAP19 that blocks specifically astrocytic Cx43 hemichannels. GAP27 mimetic peptide was also used alone to test the effect of Cx43 gap junction and hemichannel blockade on myelin integrity. Co-immunolabelling of MBP and pNF (Fig. 4A) and evaluation of myelin density and length of myelinated segments showed a decrease induced by NMO-IgG (summative data of two pools of three patients' IgG) compared to CTRL-IgG (Fig. 4B: –40%, $P < 0.001$; Fig. 4C: –32%, $P < 0.001$). But more interestingly, myelin was preserved in NMO-IgG treated condition co-treated with GAP19 (Fig. 4A). Density of myelin was not significantly reduced by NMO-IgG compared to CTRL-IgG when co-treated with GAP19 (Fig. 4B) and myelin segment length was increased by NMO-IgG with GAP19 compared to CTRL-IgG with GAP19 (Fig 4C: +27%, $P < 0.001$). By contrast, GAP27 peptide had a deleterious effect on myelin, comparable to NMO effect, inducing a drastic reduction of myelin density and myelinated segment length compared to

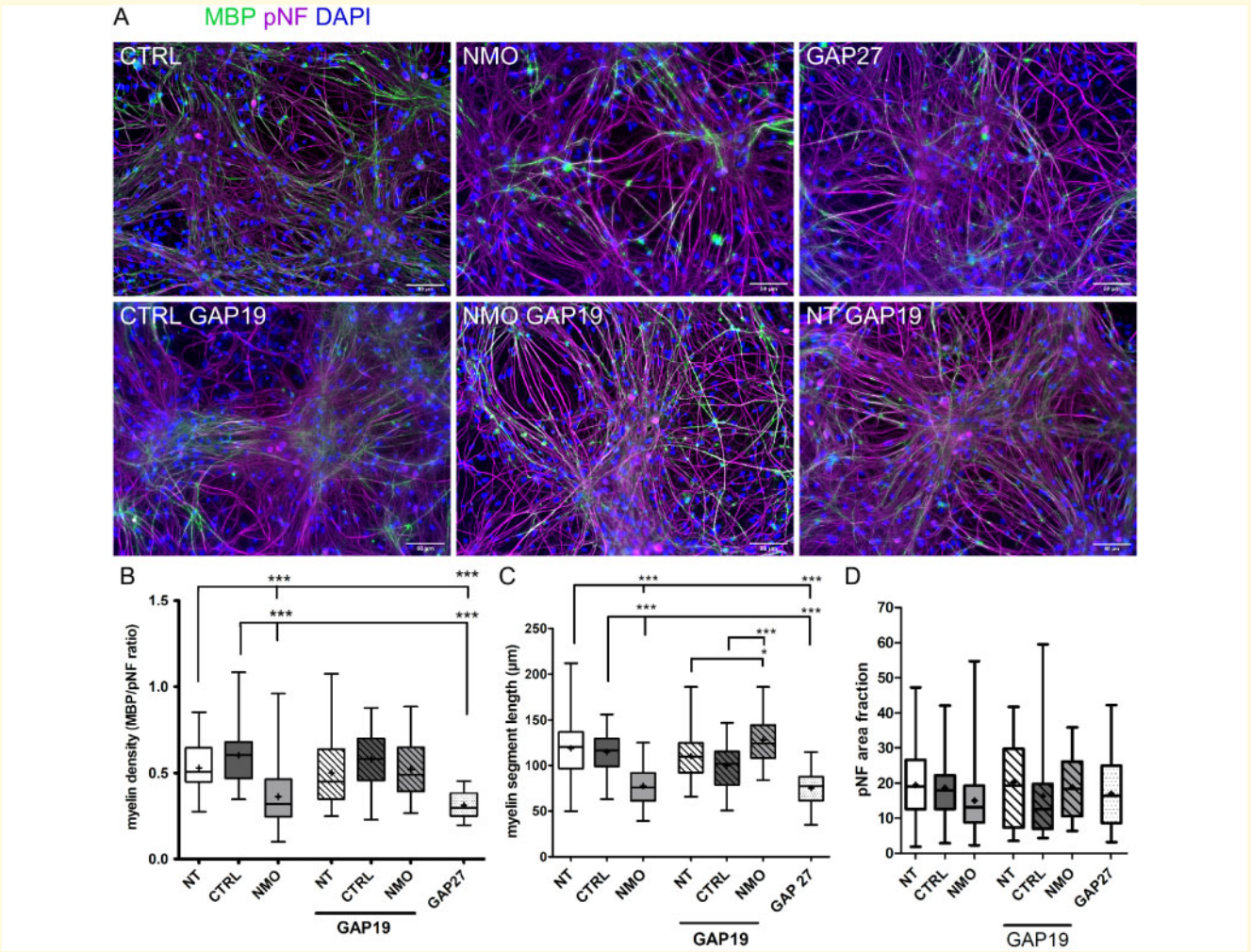

Figure 4 Modulation of Cx43 functions impacts demyelination induced by NMO-IgG. (**A**) Co-immunolabelling of axons (pNF, in magenta) and myelin (MBP, in green) on a myelinated culture at DIV28 after 48 h treatment with either no treatment (not shown), CTRL-IgG (CTRL) or NMO-IgG (NMO) and in co-treatment with the Cx43 hemichannel blocker GAP19, or treated solely with the Cx43 gap junction and hemichannel blocker GAP27. (**B**) Evaluation of myelin density showing a decrease induced by NMO (summative data of two pools of IgG from Patients NMO1–3 and NMO4–6) compared to control condition, which is prevented by a co-treatment with GAP19. (**C**) Evaluation of myelin segment length showing a decrease induced by NMO compared to control condition and an increase in NMO with GAP19 co-treatement compared to no treatment and control co-treated with GAP19 conditions. GAP27 alone strongly decreases both density and length of myelin segments compared to no treatment (**B** and **C**). (**D**) Evaluation of pNF density by the area fraction of pNF immunoreactivity showing no statistical differences between conditions. Kruskal-Wallis analysis of variances and Dunn's *post hoc* analysis $*P < 0.05$, $**P < 0.01$, $***P < 0.001$. Box and whiskers represent median with IQR and minimum maximum values, mean is represented by a plus symbol; $n = 2$ culture with each condition in duplicate.

CTRL-IgG (Fig. 4B: –49%, $P < 0.001$; Fig. 4C: –34%, $P < 0.001$). GAP19 peptide alone did not have any effect on myelin density or segment length (Fig. 4, no treatment GAP19). Quantification of axon density (pNF labelling) did not show significant differences between all conditions (Fig. 4D).

Discussion

Here we propose that that glial intercellular communication, supported by connexins hemichannels and gap junctions, are involved in the demyelination process in NMO. We showed an alteration of both expression and function of astrocytic connexins Cx43 and Cx30 in cell culture model after NMO-IgG exposure, with a rapid but transient loss of those connexins at membrane followed by an increased size of gap junction plaques. This was associated with connexin dysfunction, with decreased gap junction coupling in neuroglial syncytium, decrease of astrocytic Cx43 and oligodendrocytic Cx47 gap junctions, and increased connexin hemichannel opening. These alterations are suggested to be responsible for demyelination induced by NMO-IgG, since blocking Cx43 hemichannels with a specific peptide prevented the complement-independent demyelinating effect of NMO-IgG on myelinated culture.

There could be numerous potential mechanisms responsible for the alteration of astrocytic connexins' expression and function, induced by NMO-IgG. We found that NMO-IgG induces a quick and persistent loss of AQP4 associated with a quick reorganization of subcellular expression of Cx43 followed by increased plaque size. Thus NMO-IgG could induce a co-endocytosis of AQP4 and Cx43 and undergo lysosomal degradation (Falk *et al.*, 2014). The increased plaque size remains intriguing. However, even in large plaques, the percentage of opened channels is only up to 10–20% (Solan and Lampe, 2018). Thus, given that NMO-IgG decrease gap junction coupling, the concomitant presence of larger gap junction plaques in NMO-IgG treated culture does not reflect an increased activity. In addition, any modification of Cx43 molecular environment, notably inflammation, can affect its function. Thus, apart from direct action of NMO-IgG on AQP4, a proinflammatory environment can decrease gap junction activity and increase hemichannel activities in astrocytes (De Vuyst *et al.*, 2007; Retamal *et al.*, 2007; Orellana *et al.*, 2013). Interestingly, it has been shown that NMO-IgG can induce a specific immune response of astrocytes characterized by the activation of proinflammatory cytokines and chemokines genes (Howe *et al.*, 2014). Thus, NMO-IgG could trigger astrocytic connexin dysfunction through a proinflammatory environment. Finally, we cannot exclude that alteration of astrocytic connexins could be driven by auto antibodies not directed against AQP4 but targeting other membrane molecules, such as Cx43 itself. However, no antibodies directed against connexins were found in NMO patients with demyelinating lesions characterized by Cx43 loss and preserved astrocytes (Masaki *et al.*, 2013).

If we consider that alteration of glial connexins is implicated in the astrocyte dysfunction and concomitant demyelination in NMO, the factors responsible for demyelination remain to be identified. Many signalling molecules, such as gliotransmitters and ions, which are released by connexin hemichannels (Giaume *et al.*, 2013), can be suspected. We show here, through an EtBr uptake study, that NMO-IgG increased astrocyte hemichannel activity. This effect was blocked by carbenoxolone and would likely be blocked by GAP19 peptide as it has been shown (Abudara *et al.*, 2014). Interestingly, blocking Cx43 hemichannel activity by GAP19 peptide preserved myelin integrity in the myelinated culture treated by NMO-IgG. In addition, we show that NMO-IgG induces rapid release of glutamate from astrocytes. This idea is supported by our previous work showing the cell toxicity of molecules released by NMOIgG- treated astrocytes (Marignier *et al.*, 2010). ATP and glutamate are good candidates as they could be over-released by astrocytes with elevated Cx43 hemichannel activity, and they are known to be toxic for oligodendrocytes and myelin (Orellana *et al.*, 2013). In addition, hemichannels are activated by glutamate (De Vuyst *et al.*, 2007). The reported downregulation of glutamate transporters expression induced by NMO-IgG (Hinson *et al.*, 2008; Geis *et al.*, 2015; Marignier *et al.*, 2016) and elevated extracellular glutamate level may be a major trigger of connexin hemichannel dysfunction and have harmful effects on oligodendrocytes. By contrast, blocking Cx43 gap junction channels and hemichannels, by GAP27, had a deleterious effect on myelin integrity. The low level of hemichannel activity in basal conditions in our cellular study model suggests that GAP27 primarily blocked Cx43 gap junction activity, participating in demyelination. The loss of trophic support from astrocytes towards oligodendrocytes, as well as ions homeostasis disruption, could be also implicated in NMO-IgG-induced demyelination. In fact, not only astrocytes are coupled to one another, but they form gap junction channels with oligodendrocytes (Nualart-Marti *et al.*, 2013). Since Cx43 is essential for Cx47 expression and stability (May *et al.*, 2013), one may hypothesize that the dysregulation of Cx43 precedes that of Cx47, which could contribute to oligodendrocyte injury and demyelination. One may note that other astrocyte and oligodendrocyte connexins, notably Cx30 and Cx32, have been involved in demyelination process in multiple sclerosis (Li *et al.*, 2014; Markoullis *et al.*, 2014). We show here that the mimetic peptide GAP27, which can block Cx43 and Cx32 gap junctions (Evans and Leybaert, 2007), induced strong demyelination in the myelinated culture model, even stronger than that induced by NMO-IgG.

Although complement activation obviously plays a major role in NMO spectrum disorder pathophysiology, as recently highlighted by the dramatic effect of eculizumab on relapse prevention (Pittock *et al.*, 2019), our findings, pointing out a complement-independent astrocytopathy in NMO, are supported by robust evidences. Several *in vitro* studies found that antibody-induced AQP4 modulation led to various changes from increase blood–brain barrier permeability facilitating inflammatory cell infiltration, to water balance disruption and glutamate excitotoxicity (Marignier *et al.*, 2010; Takeshita *et al.*, 2017). Detailed study of NMO pathology showed area with astrocyte lacking AQP4 staining, in the absence of complement activation and granulocyte infiltration (Misu *et al.*, 2013; Saji *et al.*, 2013). Finally, two recent animal models of NMO support the intrinsic role of AQP4-IgG. Geis *et al.* (2015) found that repeated local administration of human AQP4-IgG can induce a potentially reversible rat spinal cord disorder; and using an intraperitoneally passive transfer of human AQP4-IgG to mice with breached blood–brain barrier, Yick *et al.* (2018) demonstrated spinal cord pathologies, including AQP4 and astrocyte loss, demyelination, and axonal injuries; both in absence of complement. However, whether these complement-independent mechanisms contribute to early development of NMOSD lesion before complement activation (Geis *et al.*, 2015; Yick *et al.*, 2018), or are associated with a more chronic deleterious effect, is still unclear. Connexinopathy could be involved at both stages. Loss of perivascular Cx43 at the astrocyte endfeet of the blood–brain barrier may increase recruitment of inflammatory cells into the CNS (Boulay *et al.*, 2015), and thus facilitate the early development of lesion formation. Astrocytic connexins dysfunction could drive the recently proposed smoldering disease process independent of clinical

attacks, responsible of continuous and sometimes deteriorating neuropsychological symptoms, including cognitive impairment (Oertel *et al.*, 2019). This inter-attack deterioration has been attributed to antibody-mediated AQP4 modulation (Saji *et al.*, 2013), as AQP4 expression plays an important role in regulating long-term synaptic plasticity (Scharfman and Binder, 2013). However, these neuropsychological symptoms could also be the consequence of prolonged connexin dysfunction. In fact, alteration of connexin may interfere with neuronal function. Astrocytes are known for their role in tripartite synapse and are part of the neuroglial network, sustained by connexins, which is crucial for synaptic plasticity and cognitive functions (Rouach *et al.*, 2008; Pannasch *et al.*, 2011; Dallérac and Rouach, 2016). Evidence of cognitive impairments in NMO patients with cortical lesions, characterized by neuronal loss but no demyelination, could involve astrocyte dysfunction, since AQP4 expression is decreased without astrocyte loss (Saji *et al.*, 2013). It would be interesting to test the effect of NMO-IgG on neuronal activity and synaptic plasticity in presence of NMO-IgG as they trigger connexin dysfunction.

Overall, our study highlights the potential crucial role of neuroglial interactions in NMO and shows how astrocytic connexin dysfunction could lead to deleterious effects on oligodendrocytes and myelin, as proposed by Cotrina and Nedergaard (2012). Prevention of demyelination by connexin inhibitors, as demonstrated on our myelinated culture model, should be further validated *in vivo*. In fact, in other diseases, treatment with connexion modulators was recently shown interesting outcomes in patients (Charvériat *et al.*, 2017). This opens modulators of connexins as a promising therapeutic alternative in neurological disorders.

Acknowledgements

We thank Nathalie Dufay from NeuroBioTec-Banques (Hospices Civils de Lyon, France) for providing Neuromyelitis Optica patients' samples and plasmaphereses, Sandrine Parrot from NeuroDialytTics plateform (Centre for Research in Neurosciences of Lyon, France) for performing extracellular glutamate dosage and Elisabeth Errazuriz and Christel Cassin from CIQLE (Centre d'Imagerie Quantitative Lyon-Est, France) for their expertise in electron microscopy.

Funding

The present study is supported by a grant from ARSEP foundation; a grant provided by the French State and handled by the "Agence Nationale de la Recherche" within the framework of the "Investments for the Future" program, under the reference ANR-10-COHO-002 Observatoire Français de la Sclérose en Plaques (OFSEP) and by a grant from "Déchaine ton Coeur" association.

Competing interests

The authors report no competing interests.

Supplementary material

Supplementary material is available at *Brain* online.

References

Abrams CK, Rash JE. Connexins in the nervous system. In: Harris AL, Locke D, editors. Connexins: a guide. Totowa, NJ: Humana Press; 2009. p. 323–57.

Abudara V, Bechberger J, Freitas-Andrade M, De Bock M, Wang N, Bultynck G, et al. The connexin43 mimetic peptide Gap19 inhibits hemichannels without altering gap junctional communication in astrocytes. Front Cell Neurosci 2014; 8: 306.

Bennett JL, Lam C, Kalluri SR, Saikali P, Bautista K, Dupree C, et al. Intrathecal pathogenic anti–aquaporin-4 antibodies in early neuromyelitis optica. Ann Neurol 2009; 66: 617–29.

Boulay A-C, Mazeraud A, Cisternino S, Saubamea B, Mailly P, Jourdren L, et al. Immune quiescence of the brain is set by astroglial connexin 43. J Neurosci 2015; 35: 4427–39.

Bradl M, Misu T, Takahashi T, Watanabe M, Mader S, Reindl M, et al. Neuromyelitis optica: pathogenicity of patient immunoglobulin in vivo. Ann Neurol 2009; 66: 630–43.

Brimberg L, Mader S, Fujieda Y, Arinuma Y, Kowal C, Volpe BT, et al. Antibodies as mediators of brain pathology. Trends Immunol 2015; 36: 709–24.

Charvériat M, Naus CC, Leybaert L, Sáez JC, Giaume C. Connexin-dependent neuroglial networking as a new therapeutic target. Front Cell Neurosci 2017; 11: 1–14.

Cotrina ML, Nedergaard M. Brain connexins in demyelinating diseases: therapeutic potential of glial targets. Brain Res 2012; 1487: 61–8.

Dallérac G, Rouach N. Astrocytes as new targets to improve cognitive functions. Prog Neurobiol 2016; 144: 48–67.

De Vuyst E, Decrock E, De Bock M, Yamasaki H, Naus CC, Evans WH, et al. Connexin hemichannels and gap junction channels are differentially influenced by lipopolysaccharide and basic fibroblast growth factor. Mol Biol Cell 2007; 18: 34–46.

Evans WH, Leybaert L. Mimetic peptides as blockers of connexin channel-facilitated intercellular communication. Cell Commun Adhes 2007; 14: 265–73.

Falk MM, Kells RM, Berthoud VM. Degradation of connexins and gap junctions. FEBS Letters 2014; 588: 1221–9.

Geis C, Ritter C, Ruschil C, Weishaupt A, Grünewald B, Stoll G, et al. The intrinsic pathogenic role of autoantibodies to aquaporin 4 mediating spinal cord disease in a rat passive-transfer model. Exp Neurol 2015; 265: 8–21.

Giaume C, Leybaert L, Naus CC, Sáez JC. Connexin and pannexin hemichannels in brain glial cells: properties, pharmacology, and roles. Front Pharmacol 2013; 4: 1–17.

Giaume C, Venance L. Intercellular calcium signaling and gap junctional communication in astrocytes. Glia 1998; 24: 50–64.

Hinson SR, Roemer SF, Lucchinetti CF, Fryer JP, Kryzer TJ, Chamberlain JL, et al. Aquaporin-4–binding autoantibodies in patients with neuromyelitis optica impair glutamate transport by down-regulating EAAT2. J Exp Med 2008; 205: 2473–81.

Hinson SR, McKeon A, Lennon VA. Neurological autoimmunity targeting aquaporin-4. Neuroscience 2010; 168: 1009–18.

Howe CL, Kaptzan T, Magaña SM, Ayers-Ringler JR, Lafrance-Corey RG, Lucchinetti CF. Neuromyelitis optica IgG stimulates an immunological response in rat astrocyte cultures. Glia 2014; 62: 692–708.

Jacob A, McKeon A, Nakashima I, Sato DK, Elsone L, Fujihara K, et al. Current concept of neuromyelitis optica (NMO) and NMO spectrum disorders. J Neurol Neurosurg Psychiatry 2013; 84: 922–30.

Kira J. Autoimmunity in neuromyelitis optica and opticospinal multiple sclerosis: astrocytopathy as a common denominator in demyelinating disorders. J Neurol Sci 2011; 311: 69–77.

Lennon VA. IgG marker of optic-spinal multiple sclerosis binds to the aquaporin-4 water channel. J Exp Med 2005; 202: 473–7.

Li T, Giaume C, Xiao L. Connexins-mediated glia networking impacts myelination and remyelination in the central nervous system. Mol Neurobiol 2014; 49: 1460–71.

Marignier R, Nicolle A, Watrin C, Touret M, Cavagna S, Varrin-Doyer M, et al. Oligodendrocytes are damaged by neuromyelitis optica immunoglobulin G via astrocyte injury. Brain 2010; 133: 2578–91.

Marignier R, Ruiz A, Cavagna S, Nicole A, Watrin C, Touret M, et al. Neuromyelitis optica study model based on chronic infusion of autoantibodies in rat cerebrospinal fluid. J Neuroinflammation 2016; 13: 15.

Markoullis K, Sargiannidou I, Schiza N, Roncaroli F, Reynolds R, Kleopa KA. Oligodendrocyte gap junction loss and disconnection from reactive astrocytes in multiple sclerosis gray matter. J Neuropathol Exp Neurol 2014; 73: 865–79.

Masaki K, Suzuki SO, Matsushita T, Matsuoka T, Imamura S, Yamasaki R, et al. Connexin 43 astrocytopathy linked to rapidly progressive multiple sclerosis and neuromyelitis optica. PLoS One 2013; 8: 1–21.

May D, Tress O, Seifert G, Willecke K. Connexin47 protein phosphorylation and stability in oligodendrocytes depend on expression of connexin43 protein in astrocytes. J Neurosci 2013; 33: 7985–96.

Misu T, Höftberger R, Fujihara K, Wimmer I, Takai Y, Nishiyama S, et al. Presence of six different lesion types suggests diverse mechanisms of tissue injury in neuromyelitis optica. Acta Neuropathol 2013; 125: 815–27.

Nicchia GP, Srinivas M, Li W, Brosnan CF, Frigeri A, Spray DC. New possible roles for aquaporin-4 in astrocytes: cell cytoskeleton and functional relationship with connexin43. FASEB J 2005; 19: 1674–6.

Niu J, Li T, Yi C, Huang N, Koulakoff A, Weng C, et al. Connexin-based channels contribute to metabolic pathways in the oligodendroglial lineage. J Cell Sci 2016; 129: 1902–14.

Nualart-Marti A, Solsona C, Fields RD. Gap junction communication in myelinating glia. Biochim Biophys Acta 2013; 1828: 69–78.

Orellana JA, Martinez AD, Retamal MA. Gap junction channels and hemichannels in the CNS: regulation by signaling molecules. Neuropharmacology 2013; 75: 567–82.

Pannasch U, Vargova L, Reingruber J, Ezan P, Holcman D, Giaume C, et al. Astroglial networks scale synaptic activity and plasticity. Proc Natl Acad Sci USA 2011; 108: 8467–72.

Pittock SJ, Berthele A, Fujihara K, Kim HJ, Levy M, Palace J, et al. Eculizumab in aquaporin-4–positive neuromyelitis optica spectrum disorder. N Engl J Med 2019; 381: 614–25.

Ratelade J, Verkman AS. Neuromyelitis optica: aquaporin-4 based pathogenesis mechanisms and new therapies. Int J Biochem Cell Biol 2012; 44: 1519–30.

Retamal MA, Froger N, Palacios-Prado N, Ezan P, Saez PJ, Saez JC, et al. Cx43 hemichannels and gap junction channels in astrocytes are regulated oppositely by proinflammatory cytokines released from activated microglia. J Neurosci 2007; 27: 13781–92.

Rouach N, Koulakoff A, Abudara V, Willecke K, Giaume C. Astroglial metabolic networks sustain hippocampal synaptic transmission. Science 2008; 322: 1551–5.

Saadoun S, Waters P, Bell BA, Vincent A, Verkman AS, Papadopoulos MC. Intra-cerebral injection of neuromyelitis optica immunoglobulin G and human complement produces neuromyelitis optica lesions in mice. Brain 2010; 133: 349–61.

Saji E, Arakawa M, Yanagawa K, Toyoshima Y, Yokoseki A, Okamoto K, et al. Cognitive impairment and cortical degeneration in neuromyelitis optica. Ann Neurol 2013; 73: 65–76.

Scharfman HE, Binder DK. Aquaporin-4 water channels and synaptic plasticity in the hippocampus. Neurochem Int 2013; 63: 702–11.

Solan JL, Lampe PD. Spatio-temporal regulation of connexin43 phosphorylation and gap junction dynamics. Biochimica Et Biophysica Acta (BBA)- Biomembranes 2018; 1860: 83–90.

Solan JL, Lampe PD. Specific Cx43 phosphorylation events regulate gap junction turnover in vivo. FEBS Lett 2014; 588: 1423–9.

Sorensen A, Moffat K, Thomson C, Barnett SC. Astrocytes, but not olfactory ensheathing cells or Schwann cells, promote myelination of CNS axonsin vitro. Glia 2008; 56: 750–63.

Su V, Lau AF. Connexins: mechanisms regulating protein levels and intercellular communication. FEBS Lett 2014; 588: 1212–20.

Takeshita Y, Obermeier B, Cotleur AC, Spampinato SF, Shimizu F, Yamamoto E, et al. Effects of neuromyelitis optica–IgG at the blood–brain barrier in vitro. Neurol Neuroimmunol Neuroinflamm 2017; 4: e311.

Thomson CE, McCulloch M, Sorenson A, Barnett SC, Seed BV, Griffiths IR, et al. Myelinated, synapsing cultures of murine spinal cord - validation as an in vitro model of the central nervous system. Eur J Neurosci 2008; 28: 1518–35.

Varrin-Doyer M, Nicolle A, Marignier R, Cavagna S, Benetollo C, Wattel E, et al. Human T lymphotropic virus type 1 increases T lymphocyte migration by recruiting the cytoskeleton organizer CRMP2. J Immunol 2012; 188: 1222–33.

Wingerchuk DM, Banwell B, Bennett JL, Cabre P, Carroll W, Chitnis T, et al. International consensus diagnostic criteria for neuromyelitis optica spectrum disorders. Neurology 2015; 85: 177–89.

Yick LW, Ma OK, Ng RC, Kwan JS, Chan KH. Aquaporin-4 autoantibodies from neuromyelitis optica spectrum disorder patients induce complement-independent immunopathologies in mice. Front Immunol 2018; 9: 1438.